NUMERICAL STUDY OF 3-D MICROSCALE HEAT TRANSFER OF A THIN DIAMOND SLAB UNDER FIX AND MOVING LASER HEATING

by

Ehsan Khalili DEHKORDI*, Afrasiab RAISI, and Behzad GHASEMI

Department of Mechanical Engineering,
Faculty of Engineering, Shahrekord University, Shaherkord, Iran

Original scientific paper
https://doi.org/10.2298/TSCI171120088D

Laser heating is one of the most practical operations in the field of solid circuit production and thin condensed film treatment. The correct prediction of the heat propagation and flux into the micro/nanothin slab under laser heating has high practical importance. Many theoretical and numerical investigations have been performed for analysis of micro/nanoheat conduction based on one or 2-D approximations. For moving laser heating of thin films, with asymmetric paths, the one or 2-D analysis cannot be applied. The most appropriate equation for micro/nanoheat transfer is the Boltzmann transport equation which predicts the phonon transport, precisely. In the present work, the 3-D microscale heat conduction of a diamond thin slab under fix or moving laser heating at very small time scales has been studied. Hence, the transient 3-D integro-differential equation of phonon radiative transfer has been derived from the Boltzmann equation transport and solved numerically to find the heat flux and temperature of thin slab. Regarding the boundary and interface scattering and the finite relaxation time in the equation of phonon radiative transfer, leads to more precise prediction than conventional Fourier law, especially for moving laser heating.

Key words: *thin solid film, laser heating, phonon radiative transfer*

Introduction

Improving the microelectronic technologies, progressing the new submicron devices and producing the solar energy harvesters are some of the considerable aspects from the application of thin condensed films. The production of smaller devices needs to fast and high quality nanotechnology methods, altering the surfaces by heat treatment and thin film processing.

One of the most important processes in the manufacturing of the micro/nanoelectronic devices is the laser surface heating. Altering the defects of the atomic structure can be made by cooling and heating of thin layers which have been investigated in many researches. The investigations of micro-nanoscale conduction heat transfer can be categorized and reviewed based on different subjects and methods of analysis which is discussed in the following.

* Corresponding author, e-mail: khaliliehsan@yahoo.com

The independence of the heat transport to the size of structure is very important in micro/nanoscle heat transfer; hence the size of thin film and boundary conditions has been studied in many previous works. Zhang *et al.* [1] analyzed the phonon heat transport in thin films using particle dynamics and studied the size effect on thermal conductivity. The lattice temperature can influence on the thermal properties and heat transfer mechanics. Slobodanka *et al.* [2] used the photo-thermal frequency method for determination of thermal properties of thin solid layers. Yang and Baleanu [3] presented a local fractional variational iteration method for the local fractional heat transfer. Han *et al.* [4] introduced the adopted lattice Boltzmann for improving the thermal conductivities of 3-D nanograins

The frequency of the lattice vibration is the other important parameter in micro/nanoscale heat conduction. Mansoor and Yilbas [5] studied the dependence of phonon radiative transport to frequency of the lattice vibration in the silicon film. They found a frequency dependent solution of phonon radiative transfer equation which resulted in the sharper decay of equivalent equilibrium temperature than that corresponding to frequency independent solution. Walther *et al.* [6] studied the oscillation behavior and safe conditions of homogenous material using the lattice Boltzmann method (LBM) for 2-D pure diffusion.

Acquiring the thermal conductivity of a thin film has been investigated in many researches. Grujicic *et al.* [7] studied the atomic-scale computations of the lattice contribution thermal conductivity of carbon nanotubes. Chen *et al.* [8] considered the effects of phonon reflection and transmission of quantum structures at the interface on the effective thermal conductivities.

The gap between two or more thin layers changes the amount of conducting heat, too. Cardona and Kremer [9] studied the temperature dependence of the electronic gaps of semiconductors and showed that the direct and indirect gaps is indispensable for optimizing the applications of semiconductors.

The Boltzmann transport equation (BTE) describes the statistical behavior of a thermodynamic system not in a state of equilibrium, devised by Ludwig Boltzmann in 1872. Many researchers have used it for the micro/nanoscale heat conduction problems. Also, the LBM is used for numerical simulations, based on the BTE. Majumdar [10] developed the 1-D equation phonon radiative transfer (EPRT) equation from the Boltzmann transport theory to analyze the 1-D heat transfer in a thin film. Joshi and Majumdar [11] studied the unsteady ballistic and diffusive phonon heat conduction on thin films. They used the BTE with relaxation time approximation and derived the EPRT and solved this equation numerically. Raisi and Rostami [12], using 1-D EPRT, studied the unsteady heat transfer across a thin film which is made of double layers of GaA and ALA. They considered diffuse scattering of phonons at the interface and determined the temperature distribution of the layers and effective thermal conductivity of structures. Yang and Chen [13] using BTE simulated the nanoscale transient heat conduction. They performed several 2-D cases and compared the results of the BTE and Fourier.

The literature review of the micro/nanoscale heat conduction is shown that there are many studies which have attempted to develop the thin solid film heat conduction. They have performed one or 2-D analysis. It is important to note that for some real engineering applications with free laser path, the one or 2-D assumption may lead to incorrect numerical predictions. Certainly, for this cases a 3-D analysis can better predict the propagation of the heat flux and the temperature of the thin solid film layer. Thus, in the present work, the transient 3-D integro-differential equation of phonon radiative heat transfer or EPRT is used to analyze the heat transfer for a thin solid film under fix and moving laser heating at both short time and

spatial scales. Also, this article concerns with finding the differences between the EPRT and Fourier results.

Problem description

Figure 1 shows a schematic of a thin diamond slab as a part of a thin film under the moving laser heating. A radial heat source with a radius, R, can start to warm the center of the bottom surface and provides a constant heat flux, q''_s, under the thin slab. Outside the radius of the heat source, there is a convection heat transfer with a fluid with, h and T_∞. Before start heating, the thin slab has a uniform temperature, T_0, as an initial condition. The analysis has been performed in two separate sections: First for the problem with fix laser source and second for the case in which the laser source translates along the Y-axis with a fix velocity under the thin slab.

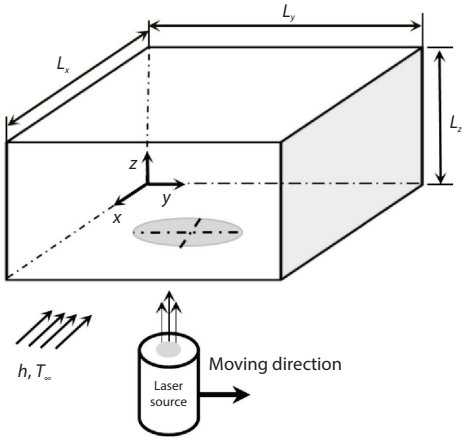

Figure 1. Schematic description for laser heating of a thin solid slab

Mathematical formulation

The general equation governing on the heat transfer is the BTE:

$$\frac{\partial f}{\partial t} + (\vec{\mathrm{v}} + \vec{\mathrm{V}}_{\mathrm{laser}})\nabla f = \left(\frac{\partial f}{\partial t}\right)_{\mathrm{scatt}} \tag{1}$$

where f, $\vec{\mathrm{v}}$, and $\vec{\mathrm{V}}_{\mathrm{laser}}$ are the distribution function, sound velocity and laser velocity, respectively. The right-hand term, scattering of the phonons, approximated by relaxation time:

$$\left(\frac{\partial f}{\partial t}\right)_{\mathrm{scatt}} = \frac{f_\omega^0 - f_\omega}{\tau_R} \tag{2}$$

where f_ω^0, τ_R, and ω are the local equilibrium distribution function, the relaxation time and the frequency of lattice vibrations, respectively. Both the Fourier law and EPRT may derive from the BTE by relative assumptions.

The 3-D form of the EPRT

Here, the derivation of the 3-D equation of phonon radiative transfer or EPRT from the BTE is explained. A Cartesian co-ordinate system is used to indicate each node with (x, y, z). The θ and ϕ are the polar and azimuthal angles for assessing the radiation direction according to the fig. 2. So, can be defined in this system as the phonon intensity:

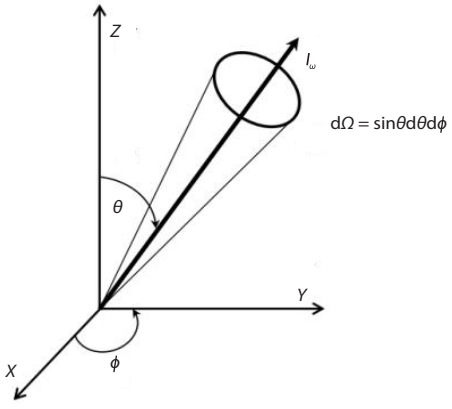

Figure 2. Schematic diagram of the co-ordinate system

$$I_\omega(\theta,\phi,x,y,z,t) = \sum_p v_p(\theta,\phi) f_\omega(x,y,z,t)\hbar\omega D(\omega) \tag{3}$$

The 3-D form of phonon intensity, I is the function of six parameters, p – is the summation is over the phonon polarization, $\hbar\omega$ – the quantum of phonon energy at a frequency ω, $D(\omega)$ – the density of states, and $\hbar$ – the reduced Planck constant. The phonon intensity must substitute to the Boltzmann equation as Majumdar [10] described the detail of it for 1-D formulation. Substituting the eq. (3) into eq. (1) the following equation is obtained:

$$\frac{1}{v}\frac{\partial I_\omega}{\partial t}+\cos\theta\frac{\partial I_\omega}{\partial z}+\sin\theta\cos\phi\frac{\partial I_\omega}{\partial x}+\left(\sin\theta\sin\phi+\frac{V_{\text{laser}}}{v}\right)\frac{\partial I_\omega}{\partial y}=\frac{I_\omega^0(T)-I_\omega}{v\tau_R(\omega,T)} \tag{4}$$

where I_ω^0 is the local equilibrium intensity distribution and it is only a function of temperature. The relaxation time, τ_R – the characteristic time for the distribution of phonons in a solid to approach the equilibrium after removing the disturbances. The local equilibrium intensity:

$$I_\omega^0=\frac{1}{4\pi}\int_{-1}^{1}\int_{0}^{2\pi}I_\omega\mathrm{d}\phi\mathrm{d}\mu \tag{5}$$

By substituting the eq. (5) into eq. (4), the final integro-differential form of EPRT:

$$\frac{1}{v}\frac{\partial I_\omega}{\partial t}+\mu\frac{\partial I_\omega}{\partial z}+\sqrt{1-\mu^2}\cos\phi\frac{\partial I_\omega}{\partial x}+\left(\sqrt{1-\mu^2}\sin\phi+\frac{v_{\text{laser}}}{v}\right)\frac{\partial I_\omega}{\partial y}=$$
$$=\frac{\frac{1}{4\pi}\int_{-1}^{1}\int_{0}^{2\pi}I_\omega\mathrm{d}\phi\mathrm{d}\mu-I_\omega}{v\tau_R(\omega,T)} \tag{6}$$

It should be noted that eq. (6) indicates the wave passes with $v(1-\mu^2)^{1/2}\cos\phi$, $v(1-\mu^2)^{1/2}\sin\phi$, and $v\mu$ speeds in the x-, y-, and z-directions, respectively. This equation illustrates that the radiated intensity waves are attenuated due to scattering represented by the right-hand side of the equations.

The heat fluxes at any point in x-, y-, and z-directions can be determined:

$$\begin{aligned}q_x''&=\int_0^{2\pi}\int_{-1}^{1}\int_0^{\omega_D}\sqrt{1-\mu^2}\cos\phi I_\omega\mathrm{d}\omega\mathrm{d}\mu\mathrm{d}\phi\\ q_y''&=\int_0^{2\pi}\int_{-1}^{1}\int_0^{\omega_D}\sqrt{1-\mu^2}\sin\phi I_\omega\mathrm{d}\omega\mathrm{d}\mu\mathrm{d}\phi\\ q_z''&=\int_0^{2\pi}\int_{-1}^{1}\int_0^{\omega_D}\sqrt{1-\mu^2}\sin\phi I_\omega\mathrm{d}\omega\mathrm{d}\mu\mathrm{d}\phi\end{aligned} \tag{7}$$

and ω_D is the Debye frequency, μ, ϕ, and ω are in the range of $-1\le\mu\le1$, $0\le\phi\le2\pi$, and $0\le\omega\le\omega_D$. After evaluation of the intensity from numerical solution of eq. (6), the temperature of any point at every time can be calculated:

$$\int_0^{\omega D}\sum_p v_p\frac{\hbar\omega D(\omega)}{\exp\left[\hbar\omega/k_BT\left(x,y,z,t\right)\right]-1}\mathrm{d}\omega=$$
$$=\frac{1}{4\pi}\int_0^{\omega_D}\int_{-1}^{1}\int_0^{2\pi}I_\omega(\theta,\phi,x,y,z,t)\mathrm{d}\phi\mathrm{d}\mu\mathrm{d}\omega \tag{8}$$

where k_B is the Boltzmann constant. Equation (8) uses the Bose-Einstein statistic as the equilibrium phonon distribution [14]. For a diamond thin slab the Debye temperature is θ_D =1860 K. The detail of calculation the Debye density of states at room temperature $D(\omega)$, was described in [15]. The physical constants of the diamond, ^{12}C, are given in tab. 1 [1].

Table 1. Physical properties of diamond [15]

Parameter	Value	Unit
Lattice constant, a	3.57	[A°]
Specific heat, C	517.05	[$Jkg^{-1}K^{-1}$]
Mass density, ρ	3510	[kgm^{-3}]
Debye temperature, θ_D	1860	[K]
Speed of sound, v	12288	[ms^{-1}]
Constant A in eq. (15)	163.94	[–]
Stefan-Boltzmann constant, k_b	50.47	[$Wm^{-2}K^{-4}$]
Number density, η	0.15410^{26}	[m^{-3}]
r in eq. (13)	1.78510^{-10}	[m]
in eq. (14)	1.58	[–]

Details of the numerical computation

The EPRT and Fourier equations are numerically solved using FORTRAN codes. The problem has been solved for transient 3-D heat conduction in a piece of diamond thin film with dimensions $L_x = L_y = L_z = 1$ μm, source heat flux $q''_s = 2.5 \cdot 10^4$ W/m^2, source radius $R = 0.2$ μm, initial temperature $T_0 = 300$ K, convection heat transfer coefficient $h = 1.5$ W/m^2, and fluid temperature $T_0 = 299$ K . For presentation of results, the appropriate dimensionless parameters have been defined. The dimensionless temperature $\theta = (T - T_0)/(q''_s L_z/K)$, dimensionless heat flux $q = q''/q''_s$, dimensionless x, y, and z lengths as $\xi_1 = x/L_x$, $\xi_2 = y/Ly$, and $\xi_3 = z/L_z$ have been used. Also, the dimensionless time has been defined as $\tau = (tv)/L_z$.

Method of finite differencing

For differentiation, the backward differencing in space has been used when the wave is traveling in the positive x-, y-, and z-directions and using forward differencing in the space when they are traveling in the negative directions. Therefore, the intensity distinguished by three superscript signs depending on the sign of μ and the range of angle, ϕ. For example:

$$0 \le \phi \le \pi/2 \begin{cases} 0 \le \mu \le 1 & I_\omega^{+++} \\ -1 \le \mu \le 0 & I_\omega^{++-} \end{cases} \qquad \pi/2 \le \phi \le \pi \begin{cases} 0 \le \mu \le 1 & I_\omega^{-++} \\ -1 \le \mu \le 0 & I_\omega^{+--} \end{cases}$$

where the superscripts indicate the positive and negative directions of x, y, and z, respectively.

Boundary and initial conditions

A brief description of the boundary conditions for the EPRT and Fourier equations is described in the following. For the EPRT, the boundary and initial conditions are defined based on the phonon intensity. For the front-back and left-right surfaces, there is the ambient temperature which causes the radiation of $I_\omega^0(T_0)$ toward the thin film on each frequency at any time:

$$I_{\omega}^{-++}(\theta,\phi,L_x,y,z,t) = I_{\omega}^{--+}(\theta,\phi,L_x,y,z,t) = I_{\omega}^{0}(T_0) \tag{9}$$

But for the bottom surface there are two separate boundary conditions. For the nodes under laser heating:

$$q_{\text{laser}} = \int_0^{2\pi}\int_{-1}^{1}\int_0^{\omega D} \mu I_{\omega}\,\mathrm{d}\omega\mathrm{d}\mu\mathrm{d}\phi \tag{10}$$

and for the outer nodes at this surface, there is a convection heat transfer:

$$q_z = h[T(x,y,z=0) - T_{\infty}] = \int_0^{2\pi}\int_{-1}^{1}\int_0^{\omega D} \mu I_{\omega}\,\mathrm{d}\omega\mathrm{d}\mu\mathrm{d}\phi \tag{11}$$

The temperature of all points at $t = 0$ is T_0. For the EPRT:

$$I_{\omega}(\theta,\phi,x,y,L_z,t=0) = I_{\omega}^{0}(T_0) \tag{12}$$

Stability criteria

For supplying the convergence, in all equations forward differencing in time was used to ensure the stability. The stability condition can be checked in the code:

$$\Delta t \le 1/\left(\left|\frac{v\mu}{\Delta z}\right| + \left|\frac{v\sqrt{1-\mu^2}\cos\phi}{\Delta x}\right| + \left|\frac{v\sqrt{1-\mu^2}\sin\phi}{\Delta y}\right|\right) \tag{13}$$

So, regarding the small size of the slab and the above criteria, the maximum of time step was calculated as $\Delta t = 8.4E - 12$ s.

Grid, spatial angles and frequency study

A structured computational grid is made for numerical solution of the EPRT. In a 3-D analysis, at each time step, the intensity matrix is dependent to six parameters. For assuring the independence of the results to the grid size, spatial angles and frequency, several numerical tests were made. In fig. 3, the dimensionless temperature belongs to the center point of the bottom face was plotted for different grids. It has no significant changes with meshes greater than (21 × 21 × 11) nodes because the calculated error is less than 0.071. Therefore, for (x, y, and z) the grid were selected with (21 × 21 × 11) nodes for the following numerical solutions. Similarly, for polar and azimuthal angles, μ and ϕ, (11 × 21) divisions were chosen. The dependence of the results to frequency leads to (41) divisions for it.

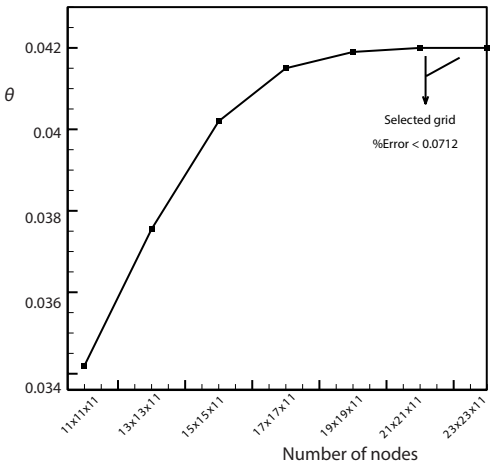

Figure 3. Dimensionless temperature of center point for bottom face *vs.* node numbers

Results and discussions

Validation

For validation of the generated EPRT code, a case for a large-scale slab, with $L_z = 1$ mm, has been solved with both the EPRT and Fourier codes. Figure 4(a) shows the dimension-

less temperature for the centerline of the bottom face (along the x-axis). Figure 4(b) compares the dimensionless temperature at the vertical centerline (along the z-axis). It is seen that there is a good agreement between the predictions of the EPRT and Fourier law in these figures. The maximum difference is seen in the bottom boundary where at dimensionless time $\tau = 1.5$, the error between two solution is less than 2.5%.

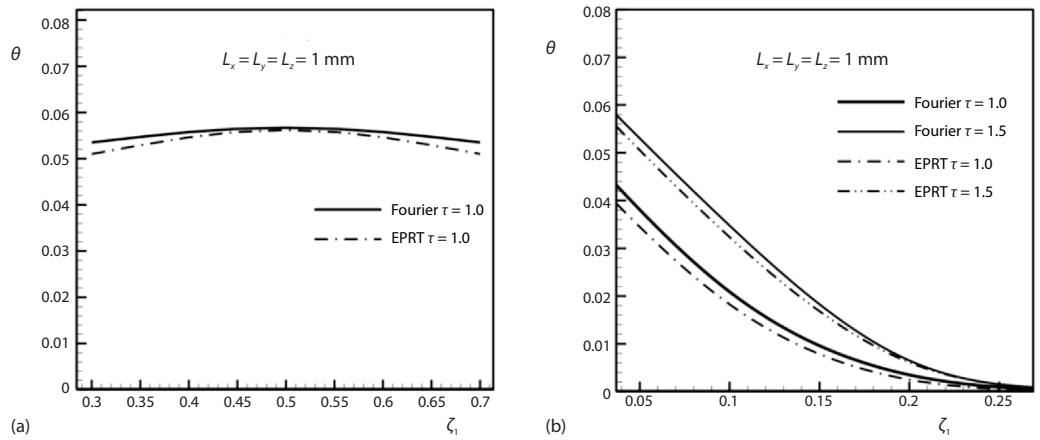

Figure 4. Validation of the EPRT code with dimensionless temperature at fix laser heating; (a) bottom center line (b) vertical center line

Fix laser heating

Figure 5 shows the isotherm contours for the bottom surface of a thin slab with $L_z = 1$ mm at dimensionless time $\tau = 1.0$ that obtained from the solution of the EPRT and Fourier equations. This figure shows that the predicted temperature by the Fourier equation is much higher than the ones belongs to the EPRT.

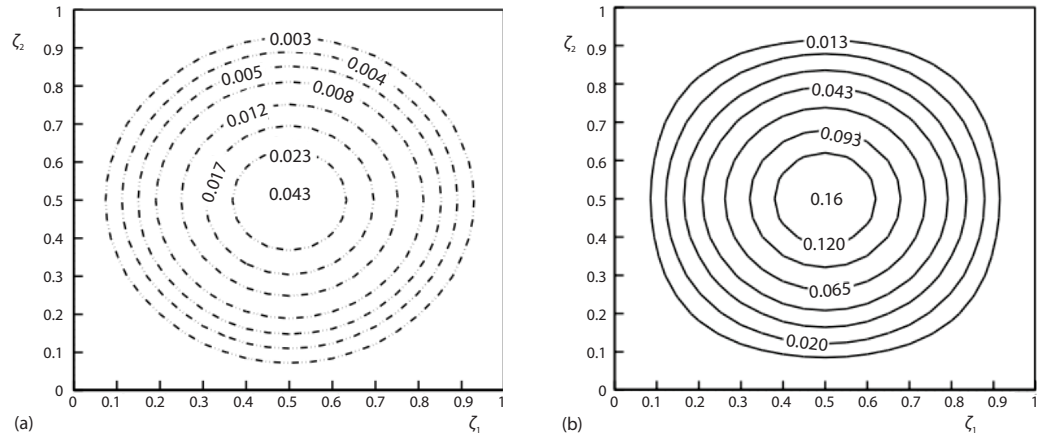

Figure 5. Fix laser heating, bottom face isotherms at $\tau = 1.0$

For a better illustration of the differences between the EPRT and Fourier prediction, the dimensionless temperature for the centerline nodes of the bottom face (along the x-axis) is plotted in fig. 6. By increasing the distance from the center of laser source, the differences between the results from both models are decreased.

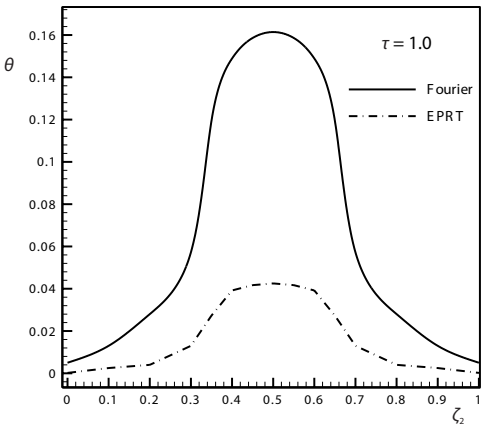

Figure 6. Fix laser heating, dimensionless temperature of the bottom face centerline at $\tau = 1.0$

It should be noted that for the present problem the dimensions of the object are in the same order of mean free path and partially ballistic heat transfer is expected. In this condition the EPRT can capture the ballistic heat transfer while the Fourier equation has a parabolic profile that propagates the energy suddenly to all nodes of the thin slab.

To show the heat penetration into the thin slab, the isotherm contours of the vertical center face (in *yz* plane) are plotted in fig. 7.

The penetration of heat into the object by the Fourier law is much faster than EPRT. Although the time is in the order of finite relaxation time and the sizes are in the order of mean free path, But the Fourier heat flux is assumed to go throw by an infinite speed. It is interesting that in the yz plane around the $y = R$ (or the heat source radius) because of scattering mechanism in the isotherm contours of the EPRT, the curves are ragged and in fact at the end points of laser radius there is a jump in temperature profiles. But, the related curves for the Fourier are completely parabolic and without any jump.

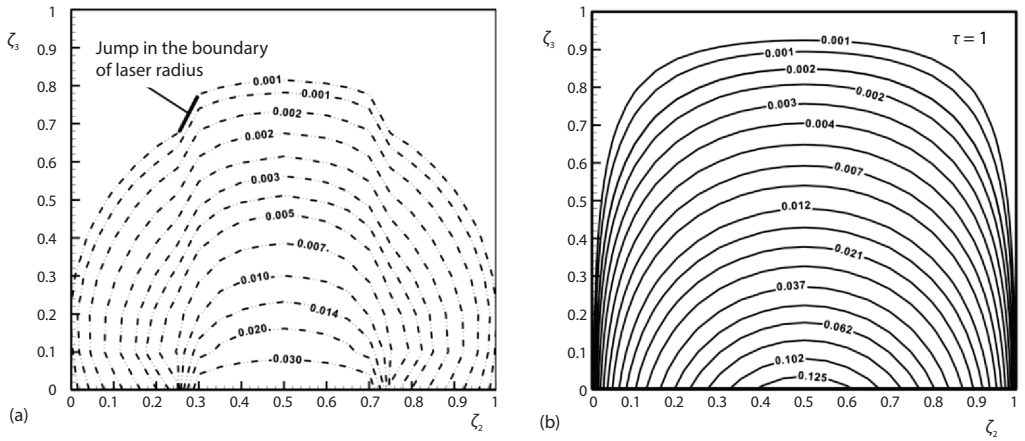

Figure 7. Fix laser heating, vertical center face isotherms at $\tau = 1.0$

Figure 8 shows the dimensionless temperature of the vertical centerline (along the *z*-axis). As shown in small scales the difference between temperature profiles obtained from EPRT and Fourier law is significant and by increment the distance from the source it decreases. Figure 9 shows a 3-D view for the propagation of the heat flux in the thin slab. Comparison the contours in four levels illustrates that the reported dimensionless temperature by the Fourier law is too much greater than the one predicted by EPRT.

Figure 10 shows the dimensionless heat flux for the vertical centerline. It is seen that the heat flux obtained from the Fourier law is higher than which from the EPRT. Note that the Fourier law uses a bulk thermal conductivity. At small scales the effective thermal conductivity is much less than the bulk thermal conductivity. Otherwise, in small time and scales, the pho-

nons have not enough chance to interact with each other and transport the energy.

Moving laser

In this section it is supposed to have a moving laser source with a constant velocity along the y axis, which is starts heating the center of the bottom face. In micro/nanoscale practical applications finding the correct temperature of the bottom face in starting time are very important. The problem is solved with the same radius and power as described in the previous section and with $V_{laser}/v = 00.3$.

Figure 11 shows the temperature contours of the bottom face at $\tau = 0.5$. It is seen that not only the Fourier predicts higher tem-

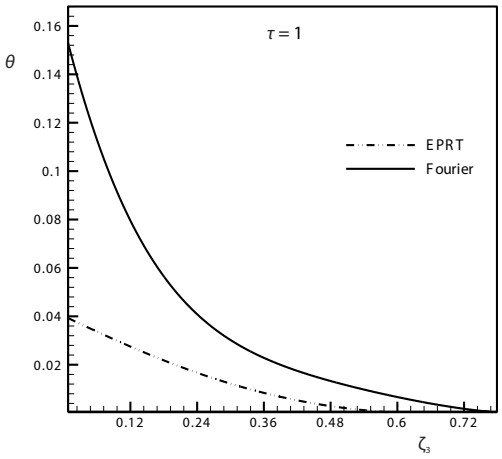

Figure 8. Fix laser heating, dimensionless temperature of vertical centerline at $\tau = 1.0$

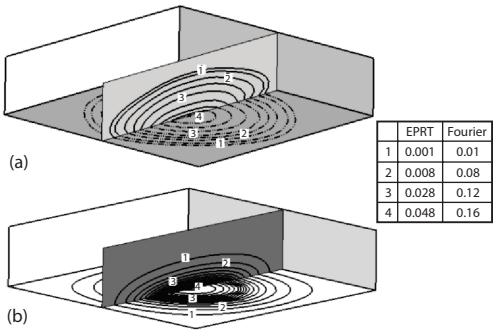

	EPRT	Fourier
1	0.001	0.01
2	0.008	0.08
3	0.028	0.12
4	0.048	0.16

Figure 9. Fix laser heating, a 3-D view of dimensionless temperature contours at $\tau = 1.0$; (a) EPRT and (b) Fourier

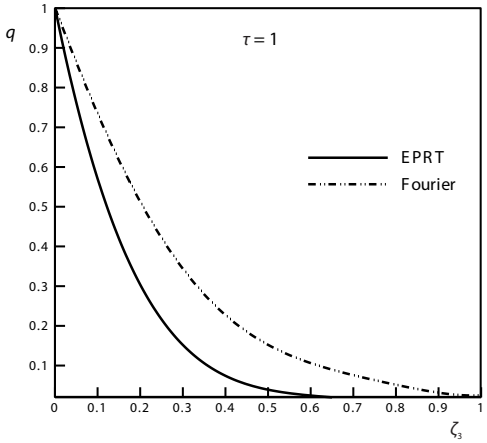

Figure 10. Fix laser heating, dimensionless heat flux at vertical centerline at $\tau = 1.0$

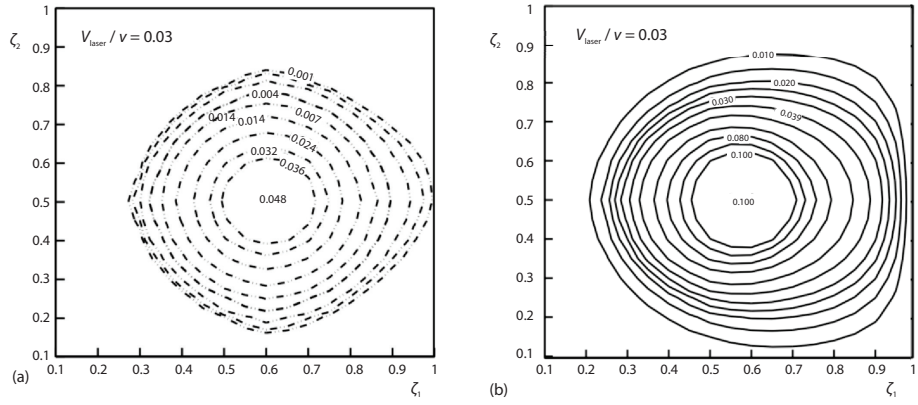

Figure 11. Moving laser heating, bottom face isotherms at $\tau = 1.0$; (a) EPRT and (b) Fourier

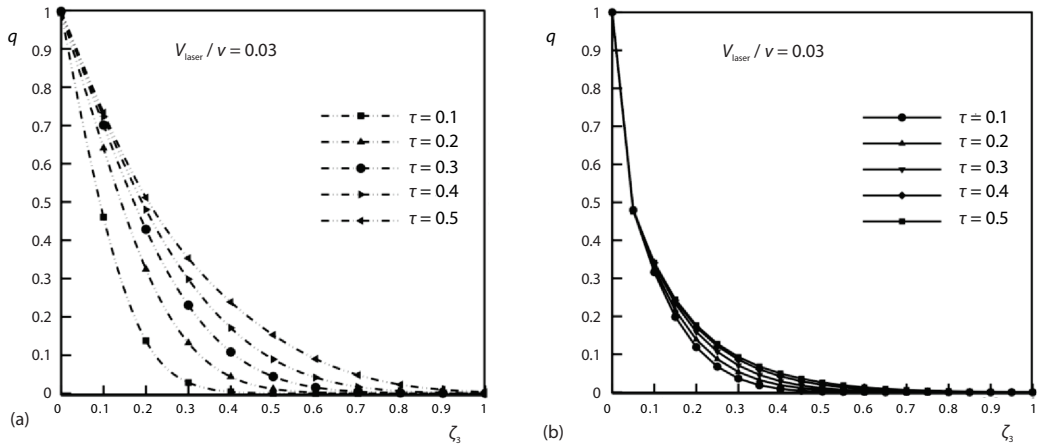

Figure 12. Moving laser heating, bottom face isotherms at $\tau = 1.0$; (a) EPRT, (b) Fourier

perature, but it also cannot capture the temperature jump in the boundary of laser radius. Using an infinite phonon speed by Fourier, as it is illustrated by Arpachi [16], leads to the heat waves propagates in the bottom face suddenly and much greater than the EPRT. It is obvious that for this case, the differences between the EPRT and Fourier predictions are more distinguishable in comparison of the fix laser case. Figure 12 compares the predicted heat flux of the EPRT and Fourier law in vertical center line. The Fourier lines are coincide with each other in the small time steps and they are not separated near the bottom face or in $\xi_3 \leq 0.1$. Also, on the other side of thin slab for $\xi_3 \leq 0.7$, the lines of predicted heat flux coincide with each other, completely. But the EPRT can distinguish the heat propagation in small time steps and the related lines are separated from each other in all small mentioned time steps.

Conclusion

Laser heating is a common process in new micro/nanostructure productions and thin solid film industries. In many ultrafast laser heating processes, the time of the process is less than the relaxation time and the size of the heated thin film is less than the mean free paths. The present work focused on the heat conduction in microscale sizes and heating time less than the relaxation time. The 3-D integro-differential EPRT was numerically solved for the transient heat conduction of a thin solid slab under fix and moving laser heating. The obtained temperature profiles and heat fluxes were compared with the Fourier law predictions, too. In small sizes and time, the predicted temperature by the EPRT was very smaller than the Fourier in different points of the thin slab. The EPRT is more powerful in prediction of the heat fluxes at very small times than the Fourier equation. It was illustrated that the difference between the EPRT and Fourier's predictions for moving laser heating is more significant than fix laser heating. The results of the unsteady 3-D present work can be applied for designing a system of heat treatment of thin solid films especially for asymmetric moving laser heating.

References

[1] Zhang, Y.-X., *et al.*, Energy Conserving Dissipative Particle Dynamics Study of Phonon Heat Transport in Thin Films, *International Journal of Heat and Mass Transfer*, *97* (2016), June, pp. 279-288
[2] Slobodanka, P.vG., *et al*., Analysis of Photo-Thermal Response of Thin Solid Films by Analogy with Passive Linear Electric Networks, *Thermal Science*, *13* (2009), 4, pp. 129-142

[3] Yang, X.-J.,Baleanu, D., Fractal Heat Conduction Problem Solved by Local Fractional variation Iteration Method, *Thermal Science*, *17* (2013), 2, pp. 625-628
[4] Han, Y.-F., *et al*., Numerical Simulation for Thermal Conductivity of Nanograin Within Three Dimensions, *Thermal Science*, *22* (2018), Suppl. 2, pp. S449-S457
[5] Mansoor, S. B., Yilbas, B. S., Phonon Radiative Transport in Silicon-Aluminum Thin Films: Frequency Dependent Case, *International Journal of Thermal Sciences*, *57* (2012), July, pp. 54-62
[6] Walther, E., *et al.*, Lattice Boltzmann Method and diffusion in Materials with Large Diffusivity Ratios, *Thermal Science*, *21* (2017), 3, pp. 1173-1182
[7] Grujicic, M., *et al.*, Atomic-Scale Computations of the Lattice Contribution Thermal Conductivity of Single-Walled Carbon Nanotubes, *Materials Science and Engineering*: *107* (2004), 2, pp. 204-216
[8] Chen, G., *et al*., Nanoscale Heat Transfer, *Encyclopedia of Nanoscience and Nanotechnology*, *7* (2004), Jan., pp. 429-459
[9] Cardona, M., Kremer, R. K., Temperature Dependence of the Electronic Gaps of Semiconductors, *Thin Solid* Films, *571*, (2014), 3, pp. 680-683
[10] Majumdar, A., Microscale Heat Conduction in Dielectric Thin Films, *Journal of Heat Transfer*, *115* (1993), 1, pp. 7-16
[11] Joshi, A. A., Majumdar, A., Transient Ballistic and Diffusive Phonon Heat Transport in Thin Films, *Applied Physics*, *74* (1993), 1, pp. 31-39
[12] Raisi, A., Rostami, A. A., Unsteady Heat Transport in Direction Perpendicular to a Double-Layer Thin-Film Structure, *Journal of Numerical Heat Transfer*, *41* (2002), 4, pp. 373-390
[13] Yang, R., *et al.*, Simulation of Nanoscale Multidimensional Transient Heat Conduction Problems Using Ballistic-Diffusive Equations and Phonon Boltzmann Equation, *Journal of Heat Transfer*, *123* (2005), 7, pp. 298-306
[14] Ashcroft, N. W., Mermin, N. D., *Solid State Physics*, Saunders College, Philadelphia, Penn., USA, 1976
[15] Kittel, C., *Introduction Solid State Physics*, 6th ed., Wiley, New York, USA, 1968
[16] Arpachi, V. S., *Conduction Heat Transfer*, Addison-Wesley Publication Company, Boston, Mass., USA, 1966

Paper submitted: November 20, 2017
Paper revised: February 22, 2018
Paper accepted: February 26, 2018